

Orbital Ordering and Spin-Ladder Formation in  $\text{La}_2\text{RuO}_5$ 

V. Eyert, S. G. Ebbinghaus, and T. Kopp

Institut für Physik, Universität Augsburg, 86135 Augsburg, Germany

(Dated: April 14, 2024)

The semiconductor-semiconductor transition of  $\text{La}_2\text{RuO}_5$  is studied by means of augmented spherical-wave (ASW) electronic structure calculations as based on density functional theory and the local density approximation. This transition has lately been reported to lead to orbital ordering and a quenching of the local spin magnetic moment. Our results hint towards an orbital ordering scenario which, markedly different from the previously proposed scheme, preserves the local  $S = 1$  moment at the Ru sites in the low-temperature phase. The unusual magnetic behaviour is interpreted by the formation of spin-ladders, which result from the structural changes occurring at the transition and are characterized by antiferromagnetic coupling along the rungs.

PACS numbers: 71.20.-b, 71.30.+h, 71.70.Ch, 71.70.Gm

Keywords: density functional theory, orbital ordering, spin-Peierls transition

The orbital degeneracy of d-shell atoms lays ground for numerous exciting phenomena observed in transition-metal compounds [1]. Orbital fluctuations as well as orbital ordering lead to extraordinary ground states, low-energy excitations and phase transitions. Well known examples for such ordering phenomena are the perovskite-based manganites [2, 3], and the antiferro-orbital structure in  $\text{KCuF}_3$  [4]. Increased complexity is observed for compounds, where the orbitals couple to the spin or charge degrees of freedom. This situation has been studied by Kugel and Khomskii for magnetic systems [5]. Orbital and magnetic ordering has also been found in the triangular chain magnet  $\text{Ca}_3\text{Co}_2\text{O}_6$ , which is characterized by an alternation of low-spin and high-spin sites [6]. In contrast, interplay of charge and orbital order as well as singlet formation has been demonstrated to play a significant role in the Magneli phase  $\text{T}_4\text{O}_7$  [7]. While orbital ordering has been primarily studied for transition-metal compounds of the 3d series, interest in the 4d oxides has considerably grown. Prominent examples for such oxides are  $\text{Ca}_2\text{RuO}_4$  [8],  $\text{Sr}_2\text{RuO}_4$ , which shows superconductivity below  $T_c \approx 1.5\text{K}$  [9], and  $\text{SrRuO}_3$ , which is ferromagnetic below  $160\text{K}$  [10].

Recently, focus has centered on the new ruthenate  $\text{La}_2\text{RuO}_5$ , which shows a first-order phase transition near  $160\text{K}$  [11]. This semiconductor-semiconductor transition is associated with a slight increase of the band gap from

$0.15\text{eV}$  to about  $0.21\text{eV}$ . In addition, it is accompanied by strong changes in the magnetic properties as well as by a transformation from a monoclinic to a triclinic lattice. High-temperature Curie-Weiss behaviour, with  $\chi_0 = 2.53\text{B}$  and  $\theta = 71\text{K}$ , is attributed to the low-spin ( $S = 1$ ) moments of the  $\text{Ru}^{4+}$  ions. At the transition, the susceptibility drops to a small, nearly temperature-independent value with a slight upturn at lowest temperatures assigned to free intrinsic spins or extrinsic impurities [11, 12]. Furthermore, from the absence of any field dependence of the magnetic susceptibility for fields up to  $9\text{T}$  a complete quenching of the magnetic moments was deduced and attributed to an orbital ordering of the Ru ions.

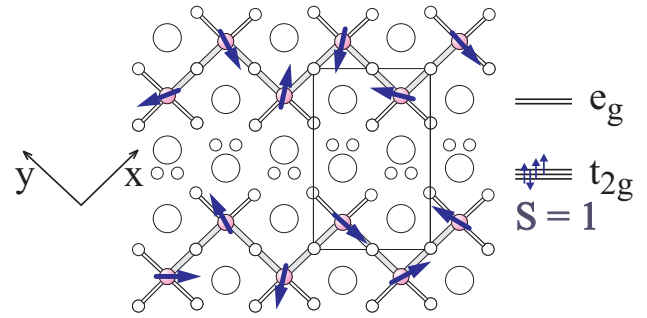


FIG. 1: Crystal structure of ht- $\text{La}_2\text{RuO}_5$  viewed along the  $c$ -direction. La, Ru, and O atoms are displayed as big, medium, and small circles, respectively.

A schematic representation of the crystal structure is displayed in Fig. 1. Arrows indicate the random orientation of the spin moments in the high-temperature (ht-) phase. The structure is built from octahedral chains parallel to the  $c$ -axis, which form a zigzag-like pattern in the  $ab$ -plane, thus giving rise to double-layer slabs, which are separated by  $\text{LaO}$ -layers [11, 13, 14]. The main features of the crystal structure are preserved in the low-temperature (lt) phase [11, 14]. However, according to the neutron data the magnetic transition is accompanied by pronounced local structural changes leading to alternating shortenings and elongations of the  $\text{Ru}\{\text{O}\}$  bond lengths [14]. While the  $\text{Ru}\{\text{Ru}\}$  nearest neighbour distances are quite similar to each other in the ht-phase, the lt-phase is characterized by short and long distances alternating both within the plane and along the  $c$ -axis. The in-plane octahedral  $\text{Ru}\{\text{O}\}$  bonds, which range from  $1.94$  to  $2.06\text{\AA}$  in the ht-phase, fall into two short and two long bonds ranging from  $1.87$  to  $1.97\text{\AA}$  and  $1.98$  to  $2.10\text{\AA}$ , respectively. The bonds parallel to the  $c$ -axis are also larger than  $2.0\text{\AA}$ . In the rotated coordinate system sketched in Fig. 1, the long and short bonds evolving in the lt-phase are along the  $x$ - and  $y$ -axis, respectively. The structural changes lead to two

inequivalent Ru sites, which alternate along the  $c$ -axis as well as the zigzag-like in-plane pattern. From structural considerations, Khalifah et al. concluded that in the  $lt$ -phase the Ru  $4d_{yz}$  orbitals are depopulated, leading to the configuration  $d_{xy}^2 d_{xz}^2 d_{yz}^0$ , hence, an  $S = 0$  state. In contrast, in the  $ht$ -phase the  $t_{2g}$  states would be nearly degenerate and Hund's rule coupling gives rise to the  $S = 1$  electron configuration of  $d_{xy}^1 d_{xz}^1 d_{yz}^1$ ,  $d_{xy}^1 d_{xz}^2 d_{yz}^1$ , or  $d_{xy}^1 d_{xz}^1 d_{yz}^2$ . Thus, the phase transition was interpreted as an orbital ordering transition with a complete loss of the local magnetic moment. Finally, the occurrence of an inelastic peak at about 40 meV as observed in neutron scattering was assigned to the formation of a spin gap in the  $lt$ -phase [11]. Underlining the importance of inter-site interactions, Osborn pointed out that the observed inelastic response should be rather attributed to singlet to triplet type excitations [15]. This point of view was supported by Khomskii and Mizokawa [16].

Concentrating on the above mentioned discrepancies in interpreting the data for the  $lt$ -phase, we report on density functional calculations as based on crystal structure data for both phases [14]. As expected, we find strong changes of the orbital occupations coming with the structural transformation. However, in contrast to the proposal by Khalifah et al., these changes conserve the local  $S = 1$  moment. From spin-polarized calculations it is inferred that the suppression of the susceptibility in the  $lt$ -phase results from a spin-Peierls-like transition coming with the formation of spin-ladders with antiferromagnetic coupling on the rungs.

The calculations were performed using the scalar-relativistic augmented spherical wave (ASW) method [17, 18]. The large voids of the open crystal structure were accounted for by additional augmentation spheres, which were automatically generated by the sphere geometry optimization (SGO) algorithm [19]. The Brillouin zone sampling was done using an increased number of up to 1024 and 2048  $k$ -points in the irreducible wedge of the monoclinic and triclinic Brillouin zone, respectively. While previous calculations (Ref. [20]) were based on the local density approximation (LDA), the present work used additionally the generalized gradient approximation (GGA) [21] as well as a new version of the ASW code, which takes the non-spherical contributions to the charge density inside the atomic spheres into account [22].

Calculated partial densities of states (DOS) are displayed in Fig. 2 for the high-temperature ( $ht$ ) and low-temperature ( $lt$ ) structure. Contributions from both Ru  $4d$  and O  $2p$  states are included. For the oxygen contributions we have distinguished the atoms O (1) to O (4), which form the  $RuO_6$  octahedra, from those of atom O (5), which is at the center of the  $La_4O$  tetrahedra. Not shown are the La  $5d$  and  $4f$  states, which give rise to a sharp peak at about 5 eV and smaller contributions between 4.5 and 1.5 eV. All other orbitals play only a negligible role in the energy interval shown.

In Fig. 2, the lowest group of bands extending from 6.9 to 1.5 eV derives mainly from the O  $2p$  states. In

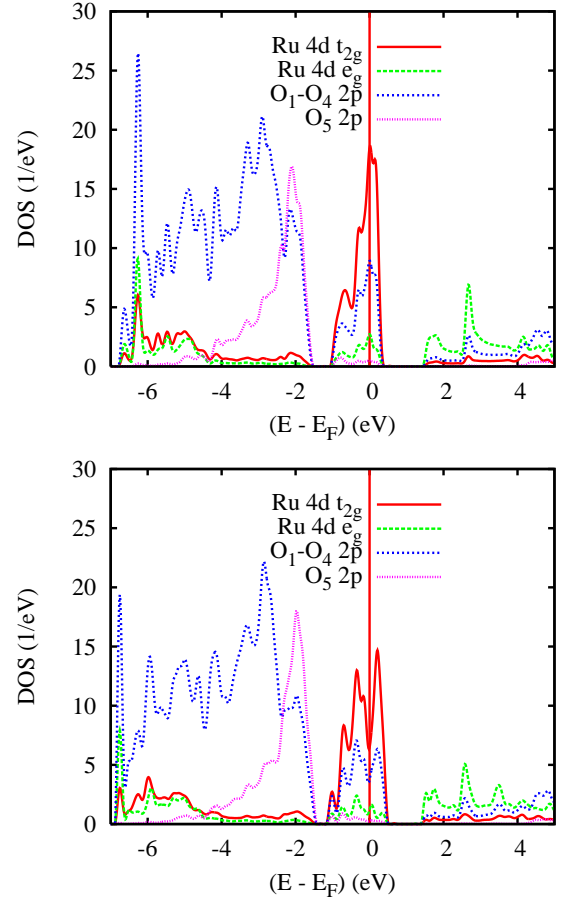


FIG. 2: Partial DOS as resulting from the  $ht$ - (top) and  $lt$ - (bottom) crystal structure.

contrast, the Ru  $4d$  states are found mainly in the energy interval from 1.1 to 0.5 eV as well as above 1.5 eV. Due to the octahedral coordination of Ru by oxygen atoms these states are split into  $t_{2g}$  bands near the Fermi energy and  $e_g$  states well above. Hybridization with the O  $2p$  states is extremely strong and leads to large admixtures to the DOS near  $E_F$ , which are of the order of 40% of the Ru  $4d$  contributions in that interval.

The partial DOS of the O (5)  $2p$  states deviates considerably from those of the remaining four oxygen atoms and shows a steady increase between 4.5 and 1.5 eV as well as a sharp drop at the upper edge. La  $5d$  and  $4f$  admixtures in this interval of the order of 15% of the O (5)  $2p$  contribution are attributed to strong hybridization coming with the formation of the  $La_4O$  (5) tetrahedra. The large bandwidth of these rather localized tetrahedral states reflects their considerable extent in space.

In general, the similarity of the crystal structures of the  $ht$ - and  $lt$ -phase is well reflected by the similarity of the partial DOS. Yet, distinct changes are observed for the Ru  $4d t_{2g}$  states. In particular, this group of bands becomes broader and the strong peak at  $E_F$ , seen for the

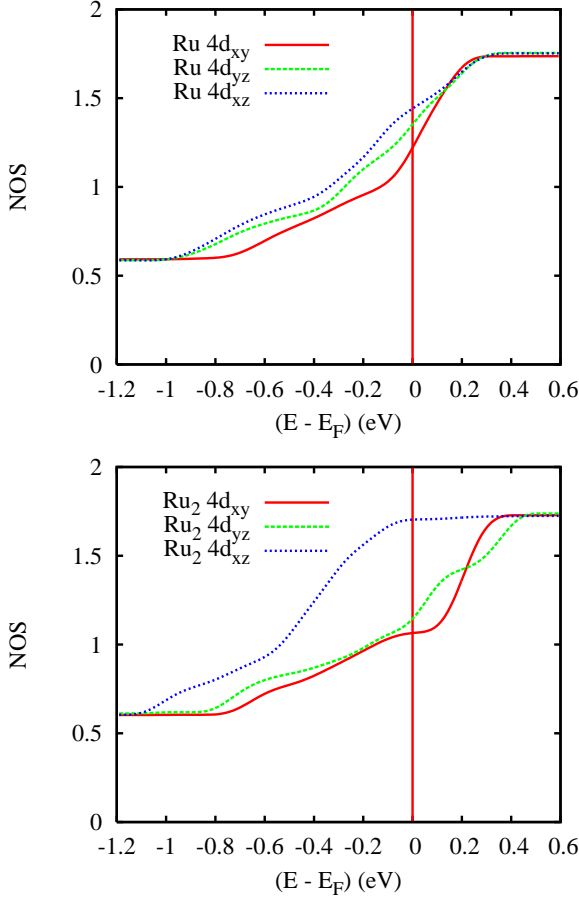


FIG. 3: Integrated partial Ru 4d  $t_{2g}$  DOS as resulting from the ht- (top) and lt- (bottom) crystal structure. Results for the Ru (1) atom of the lt-phase are very similar to those for atom Ru (2) as shown here. Orbitals refer to the rotated coordinate system depicted in Fig. 1.

ht-structure, turns into a pronounced dip. Actually, as can be seen on closer inspection of the band structure, a tiny gap is opened in the lt-phase.

The differences between the electronic properties of the ht- and lt-phase become much clearer from a detailed analysis of the near- $E_F$  states. For the notation of the orbitals the rotated coordinate indicated in Fig. 1 is used. In this system, the partial densities of states of all three Ru  $t_{2g}$  bands display the expected rather similar behaviour for the ht-phase. As a consequence, integration these partial DOS leads to almost identical orbital occupations as shown in the upper panel of Fig. 3. Note that the  $t_{2g}$  occupations do not vary from 0 to 2 in the energy interval shown as would be expected from pure d states. Due to the strong p-admixture to these bands the energy variation of the orbital occupations appears to be somewhat reduced and eventually has to be translated to the ideal picture of pure d-states. Obviously, filling the nearly degenerate  $t_{2g}$  bands according to Hund's rules leads to one of the electronic configurations  $d_{xy}^2 d_{xz}^1 d_{yz}^1$ ,  $d_{xy}^1 d_{xz}^2 d_{yz}^1$ , or  $d_{xy}^1 d_{xz}^1 d_{yz}^2$  as proposed in Ref. [11].

A noticeably different situation is obtained for the lt-structure. Integrated partial densities of states for the atom Ru (2) are shown in the lower panel of Fig. 3. The corresponding curves for atom Ru (1) are very similar and thus not displayed. Strong similarities between the  $d_{xy}$  and  $d_{yz}$  partial DOS are observed. In contrast, the  $d_{xz}$  state deviate substantially. In particular, occupation of this orbital is much larger as compared to that of the other states as is expected from the elongation of the Ru-O bonds along the local x-axis. Transferring these findings to the ideal picture of pure d states leads to the electronic configuration  $d_{xy}^1 d_{xz}^2 d_{yz}^1$ . This is in strong contradiction to the  $d_{xy}^2 d_{xz}^2 d_{yz}^0$  state proposed by Khalifah et al., who claim the full occupancy of the  $d_{xy}$  orbital at the expense of the  $d_{yz}$  state. Yet, the similar occupations of the  $d_{xy}$  and  $d_{yz}$  orbitals obtained from the present calculations are more in line with bond-length considerations using the Ru-O distances discussed above. Our results have important consequences for the magnetic moments. While Khalifah et al. propose the complete quenching of the local moment, the present calculations clearly reveal the conservation of the  $S = 1$ -spin moment through the phase transition. However, since the orbital degeneracy has been lifted by the structural distortion coming with the triclinic phase, this moment is carried exclusively by the  $d_{xy}$  and  $d_{yz}$  orbitals.

The identification of an  $S = 1$ -state for the triclinic structure motivated additional spin-polarized calculations for the lt-phase. Long-range ferromagnetic order can be ruled out from the low-temperature susceptibility data. In addition, the fact that no extra reflections were detected in the neutron diffraction data for the lt-phase allows only for antiferromagnetic order with opposite moments at the inequivalent Ru sites. This situation suggests a singlet ground state which, with the discussed structural and orbital transitions, may be realized as a spin-Peierls-like state. We have simulated this state by starting from opposite moments at the Ru (1) and Ru (2) sites. Indeed, our calculations resulted in a self-consistent solution, which comes with an energy lowering of 5 meV per Ru pair as compared to the spin-degenerate case. In addition, an optical band gap of 0.17 eV is obtained in LDA+GGA calculations result in 0.20 eV, which is very close to the experimental value.

The calculated magnetic moments arise to equal parts from the  $d_{xy}$  and  $d_{yz}$  orbitals thus confirming the expectation from the previous spin-degenerate calculations. In total, local moments of 0.77  $\mu_B$  and 0.73  $\mu_B$  are obtained at the Ru (1) and Ru (2) site, respectively. Together with small contributions from the nearest neighbour oxygen atoms a magnetic moment of 0.85  $\mu_B$  per octahedron results, which increases to 1.06  $\mu_B$  per octahedron on going from LDA to GGA. Interestingly, despite the absence of any symmetry constraint, both types of calculations lead to a compensation of the magnetic moments at neighbouring octahedra and, hence, to an exactly vanishing magnetic moment per unit cell. This finding is in excellent agreement with the suppression of the magnetic

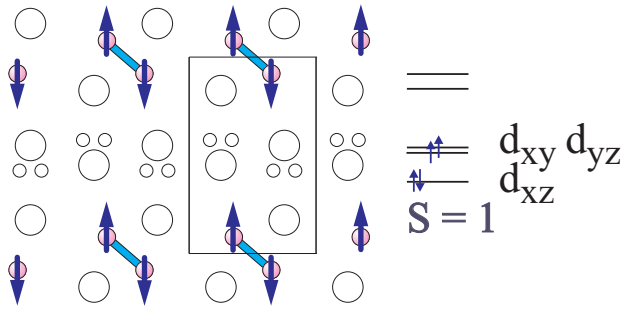


FIG. 4: Crystal and spin structure of It- $\text{La}_2\text{RuO}_5$  viewed along the  $c$ -direction. La, Ru, and O atoms are displayed as big, medium, and small circles, respectively.

susceptibility below the phase transition.

Finally, we performed spin-polarized calculations also for the ht-phase, assuming the same type of ordering as for the It-structure. As a result, a metallic solution with magnetic moments of 0.76  $\mu_B$  per Ru atom was obtained, however, with a total energy much higher than that of the corresponding spin-degenerate solution. Taking into account both the GGA and the non-spherical contributions we arrived at moments of 1.11  $\mu_B$  per Ru atom and an optical band gap of 0.02 eV. The energetical instability of this solution agrees with the fact that no long-range magnetic order is observed for the ht-

phase. The phase transition to the It-phase may thus be regarded as a spin-Peierls-like transition. Since the octahedra form chains parallel to the  $c$ -axis, the structural transformation leads to the formation of spin ladders with antiferromagnetic coupling along the rungs as indicated in Fig. 4.

To conclude, electronic structure calculations for the ht- and It-structure of  $\text{La}_2\text{RuO}_5$  reveal strong orbital ordering for the latter. While Hund's rule coupling within the degenerate  $t_{2g}$  manifold leads to a  $d_{xy}^2 d_{xz}^1 d_{yz}^1$ ,  $d_{xy}^1 d_{xz}^2 d_{yz}^1$ , or  $d_{xy}^1 d_{xz}^1 d_{yz}^2$  state in the ht-phase, the structural changes associated with the triclinic structure cause substantial orbital ordering and drive the system into a  $d_{xy}^1 d_{xz}^2 d_{yz}^1$  configuration. While well reflecting the Ru{O} bond lengths the latter preserves the local  $S = 1$  moment and thus is in contradiction with previous interpretations of the It-phase. Spin-polarized calculations for the low-temperature phase reveal compensation of the local moments due to their antiparallel alignment along the short Ru{Ru} bonds. As the formation of short and long in-plane bonds in the triclinic phase leads to an effective pairing of chains, a spin-ladder system is generated.

We are grateful to I. Leonov, J. Rodriguez-Carvajal, and C. Schuster for fruitful discussions. This work was supported by the Deutsche Forschungsgemeinschaft (DFG) through Sonderforschungsbereich SFB 484 and by the BM BF 13N 6918 (TK.).

- 
- [1] M. Imada, A. Fujimori, Y. Tokura, Rev. Mod. Phys. 70, 1039 (1998).
  - [2] A tremendous body of literature exists on this subject. An early collection of contributions can be found in: C. N. R. Rao and B. Raveau, Eds. Colossal Magnetoresistance, Charge Ordering and Related Properties of Manganese Oxides, World Scientific, Singapore (1998).
  - [3] T. Mizokawa, D. I. Khomskii, and G. A. Sawatzky, Phys. Rev. B 60, 7309 (1999); A. M. Goldman, Science 274, 1630 (1996); A. Moreo, S. Yunoki, and E. Dagotto, Science 283, 2034 (1999); Y. D. Chuang, A. Gromko, D. Dessau, T. Kimura, and Y. Tokura, Science 292, 1509 (2001); S. Elmov, V. I. Anisimov, and G. A. Sawatzky, Phys. Rev. Lett. 82, 4264 (1999).
  - [4] A. I. Liechtenstein, V. I. Anisimov, and J. Zaanen, Phys. Rev. B 52, 5467 (1995).
  - [5] K. I. Kugel and D. I. Khomskii, Sov. Phys. JETP 37, 725 (1973); Sov. Phys. Usp. 25, 231 (1982).
  - [6] V. Eyert, C. Laschinger, T. Kopp, and R. Fresard, Chem. Phys. Lett. 385, 249 (2004); R. Fresard, C. Laschinger, T. Kopp, and V. Eyert, Phys. Rev. B 69, 140405(R) (2004); H. Wu, M. W. Haverkort, D. I. Khomskii, and L. H. Tjeng, Phys. Rev. Lett. 95, 186401 (2005).
  - [7] V. Eyert, U. Schwingenschlogl, and U. Eckern, Chem. Phys. Lett. 390, 151 (2004); I. Leonov, A. Yaresko, A. N. Antonov, U. Schwingenschlogl, V. Eyert, and V. I. Anisimov, (cond-mat/0508378).
  - [8] T. Mizokawa, L. H. Tjeng, G. A. Sawatzky, G. Ghiringhelli, O. Tjernberg, N. B. Brookes, H. Fukazawa, S. Nakatsuji, and Y. Maeno, Phys. Rev. Lett. 87, 077202 (2001).
  - [9] Y. Maeno, H. Hashimoto, K. Yoshida, S. Nishizaki, T. Fujita, J. G. Bednorz, and F. Lichtenberg, Nature (London) 372, 532 (1994); T. Oguchi, Phys. Rev. B 51, 1385 (1995); D. J. Singh, Phys. Rev. B 52, 1358 (1995).
  - [10] A. Callaghan, C. W. Moeller, and R. Ward, Inorg. Chem. 5, 1572 (1966); I. I. Mazin and D. J. Singh, Phys. Rev. B 56, 2556 (1997).
  - [11] P. Khalifah, R. Osborn, Q. Huang, H. W. Zandbergen, R. Jin, Y. Liu, D. Mandrus, and R. J. Cava, Science 297, 2237 (2002).
  - [12] S. K. Malik, D. C. Kundaliya, and R. D. Kale, Solid State Commun. 135, 166 (2005).
  - [13] P. Boullay, D. Mercurio, A. Bencan, A. Meden, G. Drazic, and M. Kosec, J. Solid State Chem. 170, 294 (2003).
  - [14] S. G. Ebbinghaus, Acta Cryst. C 61, i96 (2005).
  - [15] R. Osborn, comment at the Theoretical Magnetism Meeting, July 2004.
  - [16] D. I. Khomskii and T. Mizokawa, Phys. Rev. Lett. 94, 156402 (2005).
  - [17] A. R. Williams, J. Kubler, and C. D. Gelatt, Jr., Phys. Rev. B 19, 6094 (1979).
  - [18] V. Eyert, Int. J. Quantum Chem. 77, 1007 (2000).
  - [19] V. Eyert and K. H. Hock, Phys. Rev. B 57, 12727 (1998).
  - [20] V. Eyert and S. G. Ebbinghaus, Prog. Solid State Chem.

(2006); in press.

- [21] J. P. Perdew, K. Burke, and M. Ernzerhof, Phys. Rev. Lett. 77, 3865 (1996).
- [22] V. Eyert (unpublished).